4498 *J. Phys. Chem. A* **2009,** *113,* 4498–4506

Temperature-Dependent Conformational Change of *meso*-Hexakis(pentafluorophenyl) [28]Hexaphyrins(1.1.1.1.1.1) into Möbius Structures†

Kil Suk Kim,[‡] Zin Seok Yoon,[‡] Annie Butler Ricks,[§] Jae-Yoon Shin,[‡] Shigeki Mori,[||] Jeyaraman Sankar,[||] Shohei Saito,[||] Young Mee Jung,[⊥] Michael R. Wasielewski,*[,§] Atsuhiro Osuka,*[,||] and Dongho Kim*[,‡]

Department of Chemistry, Yonsei University, Seoul 120-749, Korea, Department of Chemistry and Argonne-Northwestern Solar Energy Research (ANSER) Center, Northwestern University, Evanston, Illinois, 60208-3113, Department of Chemistry, Graduate School of Science, Kyoto University, Sakyo-ku, Kyoto 606-8502, Japan, and Department of Chemistry, Kangwon National University, Chunchon 200-701, Korea

Received: December 17, 2008; Revised Manuscript Received: February 2, 2009

At room temperature, *meso*-hexaaryl-substituted [28]hexaphyrins(1.1.1.1.1.1) in solution exist largely as an equilibrium between planar antiaromatic and distorted Möbius aromatic conformers. As the temperature decreases, the molecular structure changes into the distorted Möbius topology that commonly occurs in [28]hexaphyrins, which gives rise to longer excited singlet and triplet state lifetimes than planar antiaromatic [28]hexaphyrins. Temperature-dependent two-photon absorption measurements of [28]hexaphyrin indicate that the degree of aromaticity of Möbius [28]hexaphyrin is large, comparable to that of Hückel aromatic planar [26]hexaphyrin. Through our spectroscopic investigations, we have demonstrated that a subtle balance between the strains induced by the size of the [28]hexaphyrin macrocyclic ring and the energy stabilization contributed by π-electron delocalization in the formation of distorted Möbius [28]hexaphyrin leads to the molecular structure change into the Möbius topology as the temperature decreases.

Introduction

meso-Hexaaryl-substituted hexaphyrins(1.1.1.1.1.1) have turned out to be an attractive and representative molecule in view of aromaticity/antiaromaticity with a 26/28π electronic circuit, and reduced HOMO−LUMO gap.[1−6] Over the past few years, we have systematically investigated various photophysical properties of a series of hexaphyrins using various steady-state and time-resolved spectroscopic techniques, and quantum chemical computations.[4−6] However, among these investigations, unusual ^{1}H NMR behavior of *meso*-aryl [28]hexaphyrin(1.1.1.1.1.1), which shows a moderate diatropic ring current at room temperature in spite of a [4n] π electronic system, has remained an unsolved mystery from the viewpoint of the Hückel [4n+2] rule.[3,4]

To explain these unexpected phenomena, we have carefully considered the possibility of Möbius aromaticity, which reveals a distinct aromatic character in [4n] π electronic macrocycles by adopting a twisted Möbius topology.[7] Since Heilbronner predicted Möbius aromaticity in 1964,[8] there have been numerous research activities on Möbius aromatic molecules.[9−13] Furthermore, nowadays the search for stable Möbius aromatic molecules in the ground state has become an important effort in chemistry.

As a part of our continuing efforts to find stable Möbius aromatic molecules, we have reported the spontaneous formation of stable Möbius aromatic molecules upon metalation of expanded porphyrins including [28]hexaphyrins, [32]heptaphyrins, and [36]octaphyrins.[14] In contrast to the corresponding free base expanded porphyrins, these metalated Möbius aromatic expanded porphyrins revealed distinct aromatic character, which was confirmed by a large difference in chemical shift between the outer and inner β protons in ^{1}H NMR, large negative nucleus independent chemical shift (NICS) values (−11.4 to −14.6) and relatively large two-photon absorption (TPA) cross section values (4400−6600 GM). Additionally, the Möbius aromaticity in smaller rings of metalated N-fused [24]pentaphyrins was also characterized.[15] During the period since our work on the formation of stable Möbius aromatic expanded porphyrins through metalation and the report on di-*p*-benzihexaphyrins by Latos-Grażyński et al.,[11] increasing attention has been paid to expanded porphyrins with [4n] π electrons that have a tendency to exhibit stable Möbius aromatic character when the structure is constrained into the Möbius topology. In [4n] π-conjugated expanded porphyrins, however, the Möbius topology may necessitate a relatively large macrocyclic ring to mitigate the strains induced by molecular twisting which requires only a very small energy. Thus, “locking into a twisted Möbius topology” without an aid of additional rigidity such as metalation[14] or fusion of pyrrole rings[15] is hard to achieve. In this context, among the examples of Möbius aromatic heteroannulenic macromolecules, none of the free base expanded porphyrins have ever been reported to exhibit distinct Möbius aromaticity without any assistance of metal coordination.

Very recently, we have observed structural evidence for Möbius aromaticity in free base *meso*-aryl [28]hexaphyrin(1.1.1.1.1.1) at low temperature (~173 K).[16] The free base *meso*-aryl [28]hexaphyrin(1.1.1.1.1.1) exhibits a larger difference in chemical shift between the outer and inner β protons in its ^{1}H NMR spectra at low temperature, indicating its increased aromatic character as the temperature decreases. Moreover, two types of crystal structures for [28]hexaphyrins (planar and

---

[†] Part of the “George C. Schatz Festschrift”.

[*] Address correspondence to this author. E-mail: dongho@yonsei.ac.kr., m-wasielewski@northwestern.edu, and osuka@kuchem.kyoto-u.ac.jp.

[‡] Yonsei University.

[§] Northwestern University.

[||] Kyoto University.

[⊥] Kangwon National University.

10.1021/jp8111205 CCC: $40.75 © 2009 American Chemical Society
Published on Web 03/05/2009

SCHEME 1: Schematic Molecular Structure of *meso*-Hexakis(pentafluorophenyl) [26]Hexaphyrin(1.1.1.1.1.1) and [28]Hexaphyrin(1.1.1.1.1.1)

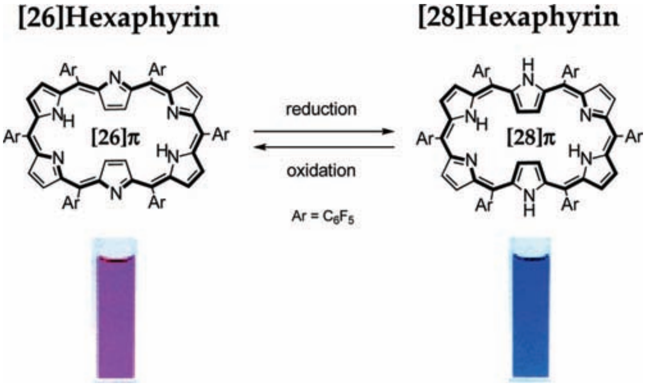

distorted Möbius topology) were obtained under different crystallization conditions. For the structure having Möbius topology, we have observed a large negative NICS value (−15.1) and significantly large HOMA values (0.71−0.85) for [28]hexaphyrin(1.1.1.1.1.1). Thus, it is likely that upon lowering the temperature the aromaticity for [28]hexaphyrins(1.1.1.1.1.1) becomes enhanced through conformational interconversion from relatively planar to single-sided Möbius structures. From this study, we were able to obtain unambiguous structural information about the conformational change of free base [28]hexaphyrin(1.1.1.1.1.1) at low temperature.

The conformational change in [28]hexaphyrins from planar to distorted Möbius geometry, or vice versa, depending on temperature, leads to a change in their electronic structures. In this regard, temperature-dependent spectroscopic studies of *meso*-aryl [28]hexaphyrins by both steady-state and time-resolved methods are indispensable to elucidate the relationship between molecular structures and photophysical properties especially in the context of Möbius aromaticity. Furthermore, from the spectroscopic point of view, free base Möbius aromatic hexaphyrins afford a definite advantage in that their photophysical properties can be exploited without perturbing the π-electronic circuitry by the presence of the central metals.

Thus, in this work, we have explored comparative temperature-dependent photophysical properties of *meso*-hexakis(pentafluorophenyl) [26]- and [28]hexaphyrins(1.1.1.1.1.1), such as singlet and triplet excited state dynamics and TPA cross-section values (Scheme 1). On the basis of our results, we have demonstrated that upon lowering the temperature the molecular structure of [28]hexaphyrin in solution strongly favors the stable and rigid, but distorted Möbius structure, which exhibits longer excited singlet and triplet state lifetimes than planar [26]hexaphyrin. In addition, we have revealed that the degree of aromaticity of Möbius [28]hexaphyrin is comparable to that of [26]hexaphyrin as examined by temperature-dependent TPA cross-section measurements.

Experimental Methods

Sample Preparations. *meso*-Hexakis(pentafluorophenyl) [26]- and [28]hexaphyrins(1.1.1.1.1.1) were synthesized according to the previously reported paper[1] and dissolved in THF solvent (Sigma-Aldrich, spectrophotometric grade).

Temperature-Dependent Experiments. For the temperature-dependent steady-state and time-resolved absorption and emission studies, a temperature-controlled liquid nitrogen cryostat (Oxford Instruments: Optistat DN) was used. The variable-temperature femtosecond transient absorption experiments were conducted by using a Janis VNF-100 cryostat with a Cryo-con 32B temperature controller. Temperatures were maintained to within ±0.05 K and allowed to equilibrate for 30 min before spectroscopic measurements.

The samples were degassed with Ar gas in order to exclude any effects from quenching reactions caused by oxygen. The results were controlled by comparison with measurements in a regular cuvette at room temperature, as possible.

Steady-State Absorption and Emission Measurements. Steady-state absorption spectra were obtained with an UV−vis−NIR spectrometer (Varian, Cary5000). For the observation of steady-state emission spectra in the near-infrared (NIR) region, a photomultiplier tube (Hamamatsu, H9170-75), a lock-in amplifier (EG&G, 5210) combined with a chopper, and a CW He−Cd laser (Melles Griot, Omnichrome 74) for the 442 nm excitation were used.

2D Correlation Spectroscopy and SMCR Analysis. Prior to PCA calculation, the mean centering operation was applied to the data matrix. To preserve the amplitude information of the variation of spectral intensities, which becomes important later for 2D correlation analysis, other steps commonly used in PCA such as normalization scaling of data according to the standard deviation were not carried out. PCA was performed in the Pirouette software package (Infometrix Inc.). Synchronous and asynchronous PCA 2D correlation spectra were obtained with the same software as described previously. Alternating least-squares (ALS) based self-modeling curve resolution (SMCR) analysis was carried out in MATLAB (Version 6, The MathWorks). To minimize the interfering noise effect in the ALS-based SMCR operation, only the two dominant principal components obtained from PCA were used to reconstruct the spectral data and the rest were truncated as noise for this study.

Femtosecond Transient Absorption Measurements. Femtosecond transient absorption measurements were performed with the following apparatus: A Spectra-Physics Millenium V frequency-doubled CW Nd:YVO_4 laser was used to pump a Coherent MIRA Ti:sapphire oscillator. The 110 fs, 832 nm pulses from the oscillator were stretched to ~200 ps by using a four-pass, reflective, single-grating pulse stretcher and were used to seed a homemade regenerative amplifier, which includes a Clark-MXR, Inc. two-step Pockels cell and driver. The amplifier was pumped at a 2 kHz repetition rate by a Quantronix 527DP frequency doubled Nd:YLF laser (4.1 mJ/pulse). The amplified Ti:sapphire pulse (0.5 mJ/pulse) was recompressed to approximately 120 fs by a four-pass, reflective, single grating compressor. The pulse energy after compression was 320 μJ/pulse. Two 5% reflective beam splitters were placed in the output path to generate two 832 nm beams for the white light generation. The remaining 832 nm light was frequency doubled by using a 1 mm type I LBO (lithium borate) crystal to give 416 nm, 120 fs, 75 μJ pulses. The 832 nm light from the first 5% beam splitter was passed through a wave plate polarizer pair to control its intensity, and a few microjoules were focused into a 1 mm sapphire disk so as to generate white light continuum pulses. All reflective optics were used both to focus the 832 nm pulse into the sapphire and recollimate the white light output, thus limiting the chirp on the white light pulse to <200 fs from 450 to 750 nm. The 832 nm light from the second 5% beam splitter was used to create a second white light continuum by focusing the 832 nm pulse into a 2 mm sapphire disk, using a 100 mm focal length (f.l.) lens. This white light was used to seed the first stage of a two-stage optical parametric amplifier (OPA) as described previously.[17] The first stage contains a type II BBO (barium borate) crystal, which was pumped with ca. 20 μJ of 416 nm light focused into the crystal with a 300 mm f.l. lens. After removal the IR idler beam and residual 416 nm pump light, the first stage produced transform-limited pulses having ~1.0 μJ/pulse from 460 to 750 nm. This light was then focused into the type I BBO of the second stage of the OPA with a 75 mm f.l. lens. The second stage amplifies the first stage light upon overlapping with the remaining 55 μJ/pulse of 416 nm pump light. The final amplified pulse energy was ~7.5 μJ/pulse after filtering the residual 416 nm and the IR idler light out. The instrument was outfitted with a CCD (Charge Coupled Device) array detector (Ocean Optics PC2000) for simultaneous collection of spectral and kinetic data. The total instrument response function (IRF) for the pump−probe experiment was 180 fs. Kinetics were determined at a given wavelength by using a nonlinear least-squares fit to a general sum of exponentials, using the Levenberg−Marquardt algorithm, while accounting for the presence of the finite instrument response.

Nanosecond Transient Absorption Measurements. Nanosecond transient absorption spectra were obtained by using nanosecond flash photolysis methods. The tunable excitation pulse was obtained from an optical paramagnetic oscillator system (Continuum, Surelite OPO) that was pumped by a Nd:YAG laser (Continuum, Surelite II-10). A CW Xe lamp (150 W) was used as a probe light source for the transient absorption measurement. After passing through the sample, the probe light was collimated and then resolved spectrally by using a monochromator with a 15 cm f.l. (Acton Research, SP150) equipped with a 600 grooves/mm grating. The light signal was detected via an avalanche photodiode (APD) (Hamamatsu, C5331−11). For the temporal profile measurements, the output signal from the APD was recorded by using a 500 MHz digital storage oscilloscope (Lecroy, WaveRunner 6050A).

Femtosecond Open-Aperture *Z*-Scan Measurement. The TPA measurements were performed by using the open-aperture *Z*-scan method with 130 fs pulses from an optical parametric amplifier (Light Conversion, TOPAS) operating at a 5 kHz repetition rate, using a Ti:sapphire regenerative amplifier system (Spectra-Physics, Hurricane). The laser beam was divided into two parts. One was monitored by a Ge/PN photodiode (New Focus) as intensity reference, and the other was used for the transmittance studies. After passing through an $f = 10$ cm lens, the laser beam was focused and passed through a quartz cell. The position of the sample cell could be varied along the laser-beam direction (z-axis), so the local power density within the sample cell could be changed under a constant laser power level. The thickness of the cell is 1 mm. The transmitted laser beam from the sample cell was then probed by using the same photodiode as used for reference monitoring. The on-axis peak intensity of the incident pulses at the focal point, I_0, ranged from 40 to 60 GW/cm. Assuming a Gaussian beam profile, the nonlinear absorption coefficient β can be obtained by curve fitting to the observed open aperture traces with the following equation:

$$T(z) = 1 - \frac{\beta I_0(1 - e^{-\alpha_0 l})}{2\alpha_0(1 + (z/z_0)^2)}$$

where α_0 is the linear absorption coefficient, l is the sample length, and z_0 is the diffraction length of the incident beam. After obtaining the nonlinear absorption coefficient β, the TPA cross-section $\sigma^{(2)}$ (in units of 1 GM $= 10^{-50}$ cm^4·s/photon·molecule) of a single solute molecule sample can be determined by using the following relationship:

$$\beta = \frac{(\sigma^{(2)} N_A d) \times 10^{-3}}{h\nu}$$

where N_A is the Avogadro constant, d is the concentration of the TPA compound in solution, h is Planck's constant, and ν is the frequency of the incident laser beam.

So as to satisfy the condition of $\alpha_0 l \ll 1$, which allows the pure TPA $\sigma^{(2)}$ values to be determined by using a simulation procedure, the TPA cross-section value of AF-50 was measured as a reference compound; this control was found to exhibit a TPA value of 50 GM at 800 nm.

Computational Method. We have calculated the molecular structures and electronic states of a series of *meso*-Hexakis(pentafluorophenyl) [26]- and [28]hexaphyrins(1.1.1.1.1.1) by DFT (density function theory; B3LYP) Hamiltonian and 6-31G* basis set by using a supercomputer (KISTI, IBM p690). The initial structures of *meso*-hexakis(pentafluorophenyl) [26]- and [28]hexaphyrins were based on the X-ray crystal structures. Additionally, we have used the SCRF (self-consistent reaction field) keyword to estimate the total energy in THF solution.

Results

Temperature-Dependent Steady-State Absorption and 2D Correlation Spectroscopy. The temperature-dependent absorption spectra of [26]- and [28]hexaphyrins in the range of 293−173 K were recorded in THF (Figure 1).

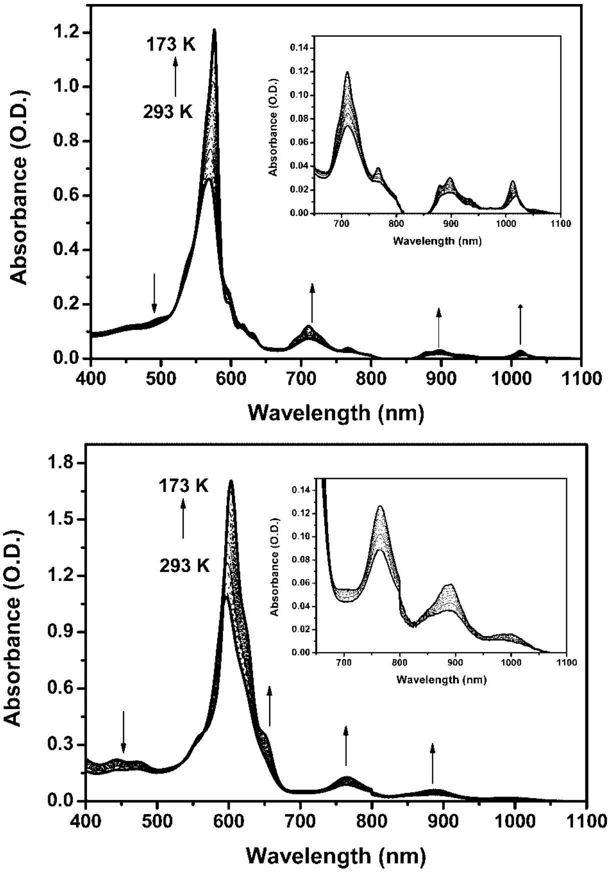

Figure 1. Temperature-dependent absorption spectra of [26]- (top) and [28]hexaphyrins (bottom) from 293 to 173 K in THF.

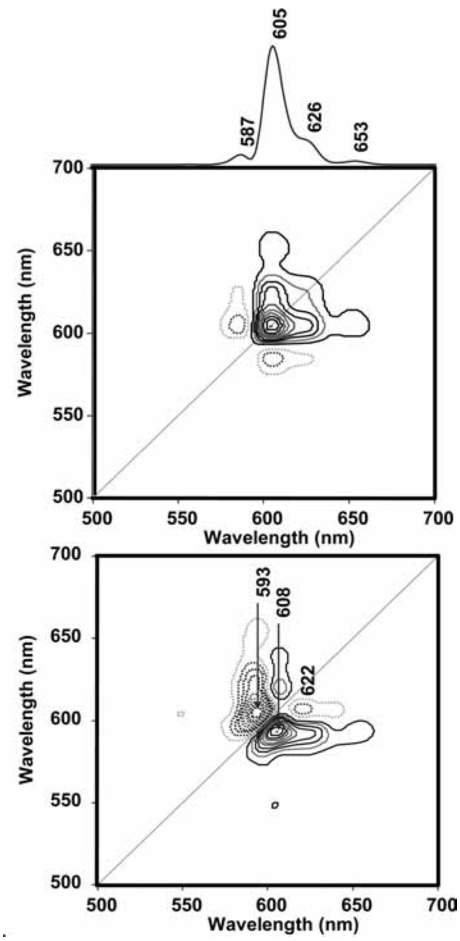

Figure 2. The synchronous (top) and asynchronous (bottom) 2D UV/vis/NIR absorption correlation spectrum generated from temperature-dependent spectral variation of [28]hexaphyrins. Solid and dashed lines represent positive and negative cross peaks, respectively.

The absorption spectra of [26]hexaphyrin show a strong B-like band at 571 nm and weaker but well-resolved Q-like ones at 712, 768, 892, and 1018 nm. On the other hand, [28]hexaphyrin exhibits a slightly asymmetric B-like band at 596 nm and relatively broad Q-like ones at 764, 847, 892, and 997 nm. Upon lowering the temperature from 293 to 173 K, [28]hexaphyrin shows a red-shift in the B-like band from 596 to 605 nm (250 cm^{-1}), accompanied by spectral changes such as an appearance of a shoulder at ~650 nm, while [26]hexaphyrin exhibits only a slight peak shift in the B-like band from 571 to 575 nm (122 cm^{-1}).

To find out the origin for the spectral changes in the absorption spectra of [28]hexaphyrin with a decrease in temperature, we have adopted a consistent 2D correlation spectroscopic analysis, a technique where the spectral intensity is plotted as a function of two independent spectral variables, which can provide specific information on conformational changes depending on temperature.[18] Synchronous and asynchronous 2D correlation spectra were calculated by using the algorithm developed by Noda.[19] The band at 605 nm in the synchronous spectrum was separated into two independent bands in the asynchronous spectrum, 593 and 608 nm (Figure 2). This 2D correlation analysis strongly implies that [28]hexaphyrin exists as at least two conformers in the ground state. Furthermore, the relative intensity ratio between the two bands at 593 and 608 nm shows temperature-dependent behavior, where the band at 593 nm becomes dominant at higher temperature but the one at 608 nm is more intense at lower temperature.

To evaluate the absorption spectral changes and their corresponding concentration profiles of individual [28]hexaphyrin conformers during temperature change, we adopted a self-modeling curve resolution (SMCR) analysis (see Figure S1 in the Supporting Information (SI)). Jung et al.[20] have introduced the use of 2D correlation spectroscopy in conjunction with alternating least-squares (ALS)-based SMCR analysis of the spectral data set to obtain the concentration profiles and spectral changes of pure chemical species from the unknown spectra of a mixture without prior knowledge about the system. Through the SMCR analysis of the temperature-dependent absorption spectra of [28]hexaphyrin, we can extract the two ground state absorption bands contributed by two conformers. One reveals a B-like band at 604 nm and distinct Q-like bands at 764, 890 nm, and the other one shows a relatively blue-shifted B-like band at 589 nm and featureless Q-like bands. In general, the absorption spectra of aromatic expanded porphyrin molecules appear with intensified and distinct Q-transition bands. On the other hand, the absorption spectra of antiaromatic expanded porphyrin molecules have no distinct Q-bands or only smeared (weak) Q-bands in their absorption spectra.[21,22] In this regard, we can assume that the two absorption spectra revealed by the SMCR analysis are responsible for planar Hückel and distorted Möbius aromatic [28]hexaphyrin conformers existing in equilibrium. In addition, through the SMCR analysis, we were able to obtain the temperature-dependent relative population change of the two conformers (Figure S1 in the SI). As the temperature decreases, the simulated relative population ratio of Möbius aromatic [28]hexaphyrins increases from 55% to 75%, while that of planar antiaromatic ones decreases from 45% to 25%, which suggests that the population of Möbius aromatic [28]hexaphyrins gradually increases at the expense of planar antiaromatic [28]hexaphyrins in the ground state as the temperature decreases.

Temperature-Dependent Fluorescence Spectra. The fluorescence spectra of [26]- and [28]hexaphyrins were obtained by using the 442 nm excitation line of a He−Cd laser in the range of 293−173 K (Figure 3).

The fluorescence spectra of [26]- and [28]hexaphyrins show intense peaks at 1032 and 1034 nm, and weaker vibronic bands around 1250 nm. The bandwidths of the intense fluorescence peaks of [26]- and [28]hexaphyrins were estimated to be ~330 and ~700 cm^{-1}, respectively, by assuming a single Gaussian component. As the temperature decreases, the fluorescence spectra of [26]- and [28]hexaphyrins become sharpened, blue-shifted, and intensified. However, the variations in Stokes shifts and relative fluorescence quantum yields between [26]- and [28]hexaphyrins show quite different behaviors.

Considering the lowest Q-like absorption bands, the Stokes shifts of [26]- and [28]hexaphyrins were estimated to be ~133 and ~358 cm^{-1} at 293 K, respectively. The Stokes shifts of [26]hexaphyrin become slightly smaller from 133 to 108 cm^{-1} (ca. 25 cm^{-1}) as the temperature decreases from 293 to 173 K, whereas those of [28]hexaphyrin change more significantly from 358 to 254 cm^{-1} (ca. 104 cm^{-1}) (Figure S2 in the SI). These results suggest that the structural changes in the S_1 state relative to the ground state are larger for [28]hexaphyrin than those for [26]hexaphyrin.

The relative fluorescence quantum yields (Φ_f) of [26]- and [28]hexaphyrins show interesting features (see Figure S2 in the SI). To evaluate the relative Φ_f, we have assumed the fluorescence quantum yields of [26]- and [28]hexaphyrins at 173 K are unity. For [28]hexaphyrin, the decreasing ratio in Φ_f of [28]hexaphyrin with temperature is larger than that of

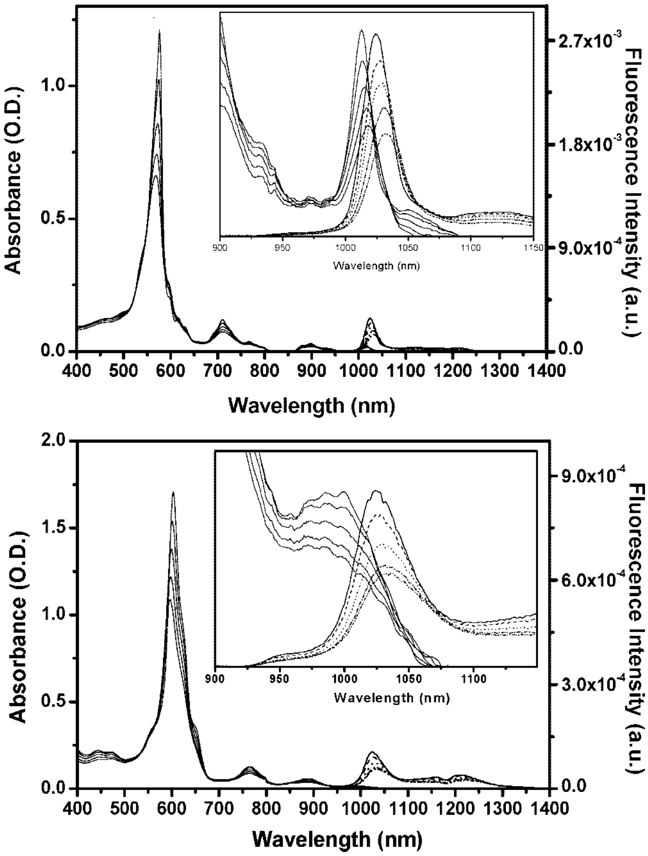

Figure 3. Temperature-dependent absorption and fluorescence spectra of [26]- (top) and [28]hexaphyrins (bottom) excited by the 442 nm line of a He−Cd laser at 293, 263, 233, 203, and 173 K in THF.

TABLE 1: Singlet and Triplet (π, π*) Excited State Lifetimes of [26]- and [28]Hexaphyrins in Temperatures from 293 to 173 K

temp	[26]hexaphyrin		[28]hexaphyrin		
(K)	τ_{S_1} (ps)[a]	τ_{T_1} (μs)[b]	τ_{S_1} (ps)[c]	τ_{S_1} (ps)[d]	τ_{T_1} (μs)[e]
293	113	4.8	183	17 (30%), 210 (70%)	<0.1
273	121	5.8	179	17 (17%), 246 (83%)	0.15
253	126	6.5	203	17 (19%), 269 (81%)	0.3
233	137	8.7	223	17 (15%), 232 (85%)	1
213	138	10.5	250	17 (10%), 243 (90%)	7
193	139	10.9	250	250	30
173	140	11.9	260	260	90

[a] Excitation and probe wavelengths: 563 nm, 575 nm. [b] Excitation and probe wavelengths: 567 nm, 530 nm; obtained under the Ar gas saturated condition. [c] Excitation and probe wavelengths: 594 nm, 616 nm. [d] Excitation and probe wavelengths: 594 nm, 638 nm. [e] Excitation and probe wavelengths: 607 nm, 650 nm; obtained under the Ar gas saturated condition.

[26]hexaphyrin [-3.6×10^{-3}/K vs. -1.75×10^{-3}/K], supporting the existence of various conformers at high temperature.

Temperature-Dependent Singlet and Triplet Excited State Dynamics. To explore the excited state conformational dynamics of [26]- and [28]hexaphyrins depending on temperature, we have carried out femtosecond and nanosecond transient absorption experiments in the range of 173−293 K in THF (Table 1, Figure 4, and Figure 5).[23]

The femtosecond transient absorption spectra of [26]- and [28]hexaphyrins exhibit strong bleaching signals of the B-like bands at 565 and 605 nm and relatively weak induced absorption bands on both sides of bleaching bands, respectively. The decay profiles of [26]hexaphyrin at 575 nm can be fitted to a single exponential function and only slight changes in lifetimes occur from 110 to 140 ps upon lowering the temperature. On the other hand, [28]hexaphyrin reveals a probe wavelength dependence. In this case, upon lowering the temperature, the decay profiles probed at 616 nm can be fitted to a single exponential function with the decay time constant increasing from 183 to 260 ps, but the decay profiles probed at 638 nm could not be fitted to a single exponential function and were better fitted to biexponential decays with the time constants of ∼17 ps (30%) and ∼210 ps (70%) at 293 K (see Table 1, as well as Figure S3 in the SI). Interestingly, as the temperature decreases, the contribution by the short decay component gradually decreases from 30% to 10%, while the long decay component increases from 70% to 90%, and below 193 K, the single exponential decay fitting with the 250−260 ps time constant was possible. The increasing portion of longer time constant with the expense of the decreasing portion of the shorter one upon lowering the temperature seems to be correlated with the temperature-dependent SMCR analysis. That is, the short and the long decay time constants might indicate the mixture of Hückel antiaromatic and Möbius aromatic conformers, respectively.

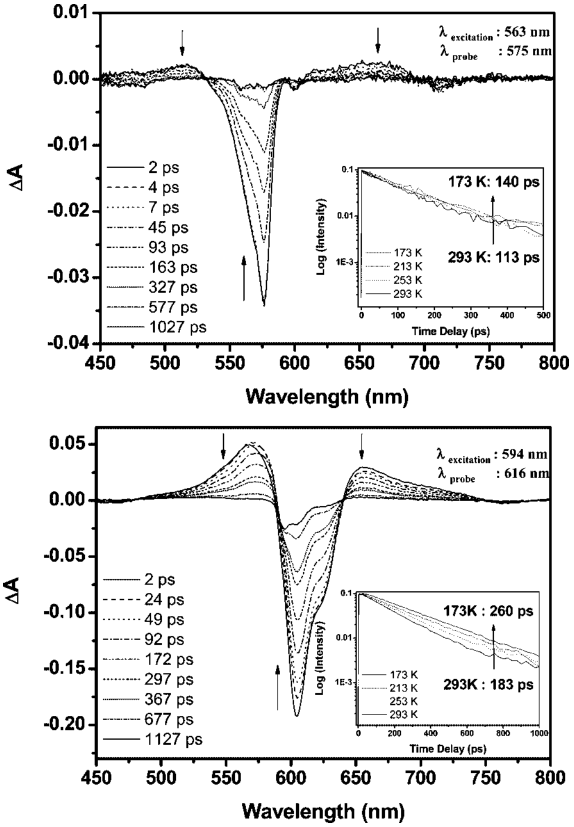

Figure 4. Femtosecond transient absorption spectra of [26]- (top) and [28]hexaphyrins (bottom) in THF at 173 K. The inset shows the temperature-dependent S_1 state kinetic profiles from 293 to 173 K in THF.

To support this assumption, we controlled the excitation wavelengths of [28]hexaphyrin through 580 and 620 nm pump wavelengths at 293 K (see Figure S4 in the SI). At each excitation wavelength, the decay profile probed at 616 nm showed the single exponential behavior (∼200 ps), while that at 580 nm showed the biexponential decays with the time constants of ∼17 and ∼200 ps. It should be noted that the contribution of short component (44%) pumped at 580 nm is larger than that (22%) at 620 nm. In our previous work, it has been demonstrated that the singlet excited states of antiaromatic

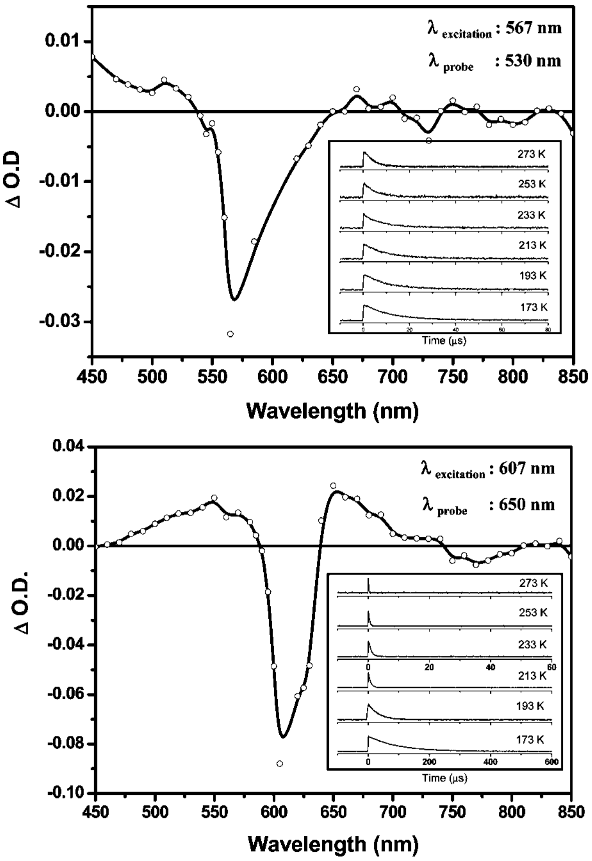

Figure 5. Nanosecond flash photolysis spectra of [26]- (top) and [28]hexaphyrins (bottom) in THF at 173 K. The sample was degassed with argon gases. The inset shows the temperature-dependent T_1 state decay profiles from 273 to 173 K.

expanded porphyrins exhibit the time constants of only a few tens of picoseconds or less compared to their aromatic congeners.[5,24−26] In this context, we can assign the short decay time constant of ~17 ps to the S_1 (π,π^*) state lifetime of planar Hückel antiaromatic [28]hexaphyrin and the relatively long component to the distorted Möbius aromatic [28]hexaphyrin.

In the same manner, we have carried out nanosecond flash photolysis experiments of [26]- and [28]hexaphyrins in the range of 173−293 K under an Ar-saturated THF solution with the excitation wavelengths of 567 and 607 nm, respectively (Figure 5).[27]

Similar to the femtosecond transient absorption spectra, [26]- and [28]hexaphyrins showed strong bleaching and induced absorption signals in the nanosecond flash photolysis experiment (Figure 5). The temperature-dependent kinetics for [26]- and [28]hexaphyrins were monitored at 530 and 650 nm, respectively. At 293 K, the T_1 state lifetime for [26]hexaphyrin was estimated to be ca. 4.8 μs, while that for [28]hexaphyrin it could not be determined presumably due to very short lifetime of its T_1 state (<100 ns). On the other hand, as the temperature decreases, the T_1 state lifetimes for [28]hexaphyrin show a larger change (from ~0.1 to 90 μs) than that for [26]hexaphyrin (from 4.8 to 11.9 μs), similar to the excited state dynamics shown by femtosecond transient absorption measurement.

Consequently, these singlet and triplet excited state dynamics clearly reflect the temperature-dependent conformational interconversion dynamics between Möbius aromatic and Hückel antiaromatic [28]hexaphyrins, which is consistent with the results in the SMCR analysis, Stokes shifts, and the relative fluorescence quantum yields.

Temperature-Dependent Two-Photon Absorption Cross-Section Values. The congeneric nature of [26]- and [28]hexaphyrins permits us to explore in greater depth the correlation between the two-photon absorption (TPA) cross-section values and the observed aromaticity. To gain further insight into the aromaticity based on Hückel's [$4n+2$] rule of π-conjugated molecular systems, we have measured the temperature-dependent TPA cross-section values of [26]- and [28]hexaphyrins using a femtosecond *Z*-scan method (Figure 6).[28]

We have selected the two-photon excitation wavelengths where the one-photon absorption contribution to the two-photon absorption could be ignored. As expected, [26]hexaphyrin shows much larger TPA cross-section values (~10^4 GM) at room temperature, compared with its congener [28]hexaphyrin (~2100 GM).[4,5] The larger TPA cross-section value in [26]hexaphyrins can be considered to reflect an increased diatropic ring current relative to [28]hexaphyrin at room temperature. In the case of [26]hexaphyrins, as the temperature decreases, the TPA cross-section values of 9000−10000 GM remain nearly constant regardless of temperature, indicating that there is little conformational change depending on temperature as seen in the temperature-dependent NMR experiments. In sharp contrast, the TPA cross-section value of ~2100 GM in [28]hexaphyrin at room temperature gradually increases to ~9100 GM upon lowering the temperature to 173 K, which is almost comparable to that of [26]hexaphyrin. Thus, the temperature-dependent TPA data of [28]hexaphyrin are in excellent agreement with the temperature-dependent NMR data, showing that the conformational dynamic nature of [28]hexaphyrin between Möbius aromatic and planar rectangular (thereby antiaromatic) conformations is completely frozen at 173 K. In addition, these results are well-correlated with femtosecond and nanosecond transient absorption experiments. Thus, in parallel with the variable-temperature NMR data, the temperature-dependent TPA cross-section values also clearly demonstrate the fast equilibrium processes between the two conformers in [28]hexaphyrin at room temperature, which is frozen with a predominant distribution of Möbius aromatic [28]hexaphyrin at 173 K.

Discussion

The absorption spectra of [26]- and [28]hexaphyrins in solution at 293 K are quite similar to each other except for the absorption peak positions. According to our recent studies on bis-gold(III) [26]- and [28]hexaphyrins[21,22] which exhibit general Hückel aromatic and antiaromatic character respectively in their ^{1}H NMR spectra, the absorption spectra of Hückel aromatic bis-gold(III) [26]hexaphyrins exhibit intense and distinct Q-like bands. On the other hand, Hückel antiaromatic bis-gold(III) [28]hexaphyrins have no distinct but only smeared Q-like bands in their absorption spectra.[21,22] In this context, while the absorption spectra of [26]hexaphyrin seem to reflect Hückel aromatic character, those of [28]hexaphyrin do not represent typical Hückel antiaromatic character. Therefore, the overall absorption spectra of [28]hexaphyrin are attributable to the combination of accessible [28]hexaphyrin conformers (planar and distorted Möbius topology).

To delineate the conformational dynamics of [28]hexaphyrin more quantitatively, we have estimated the activation energy barrier for the conformational change between planar and distorted conformers in the ground state. To estimate the activation energy barrier for [28]hexaphyrin conformational isomerism, we have adopted a temperature-dependent dynamic NMR method.[29] When the conformational interconversion processes are slower than NMR time scale at low temperature,

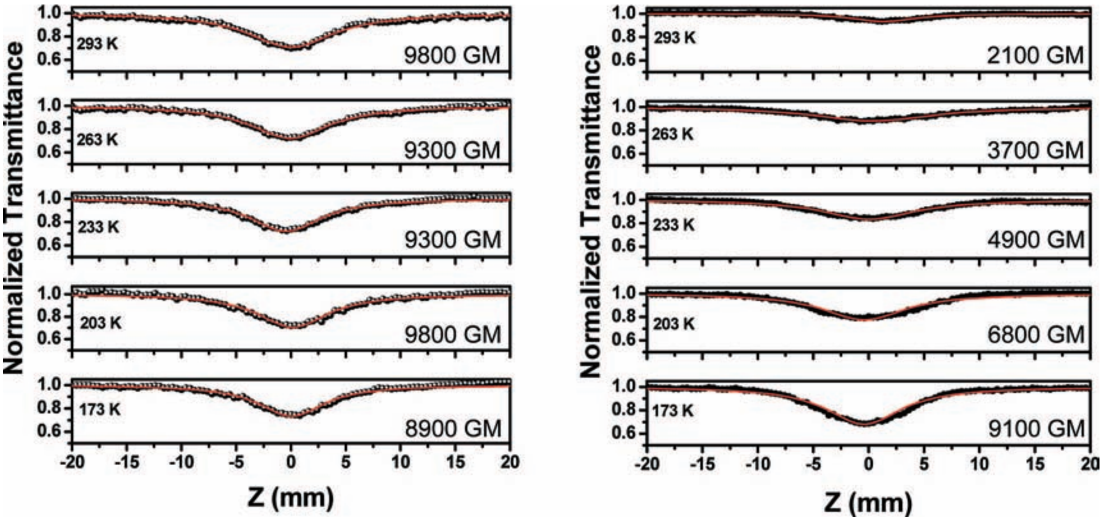

Figure 6. The open aperture *Z*-scan trace for [26]- (left) and [28]hexaphyrins (right) in THF under variable temperature with excitation at 1200 nm. The sample concentration for [26]- and [28]hexaphyrins is 0.3 and 0.5 mM, respectively. The red lines are the best fitted curves of experimental data.

the NMR spectrum shows two distinct sets of signals for two individual nuclei. As the temperature increases, these processes reach the NMR time scale, at which the peaks become gradually broadened and show coalescent spectral shapes. Finally, when these processes are faster than the NMR time scale at higher temperature, the NMR shows only a single narrow line at the central position between the two chemical shifts obtained in the slow interconversion rate at low temperature. In this sense, the temperature-dependent NMR spectra of [28]hexaphyrin show clear evidence of the conformational interconversion processes. In reality, the ^{13}C NMR spectra of [28]hexaphyrin reveal two sets of signals at 98 and 106 ppm at 173 K, which broaden and coalesce at higher temperature, but only a single narrow peak shows up at 102 ppm at 293 K. The ^{1}H NMR spectra of [28]hexaphyrin also show a similar phenomena in the same temperature range (see Figures S5 and S6 in the SI). Through an analysis of these NMR spectral changes, we can obtain the interconversion rate constants (k_{int}) between the two [28]hexaphyrin conformers, and thus the Arrhenius plot of ln k_{int} vs. $1/T$ gave the activation energy barrier, which was estimated to be 8 ± 1 kcal/mol.

Furthermore, we have obtained the theoretical total energy difference between planar and distorted Möbius [28]hexaphyrins by including all six pentafluorophenyl substituents using the Gaussian 03 package (see Figure S7, SI).[30] Since all the spectroscopic measurements were carried out in THF, we have considered the effect of solvent in calculating the ground state energy of [28]hexaphyrin by assuming a dielectric medium based on the Onsager model for better comparison. As a result, the total energy of Möbius aromatic [28]hexaphyrin was estimated to be more stable by ~3.7 kcal/mol than planar antiaromatic [28]hexaphyrin. Thus, considering the activation barrier energy of 8 ± 1 kcal/mol as well as the ground state energy difference of ~3.7 kcal/mol in THF between the two conformers, we think that the population of the more stable conformer, which is believed to be Möbius aromatic [28]hexaphyrin, increases gradually as the temperature decreases.

On the basis of the temperature-dependent steady-state and time-resolved spectroscopic results, we can propose the energy relaxation pathways for [26]- and [28]hexaphyrins at 293 and 173 K (Figure 7).

In the case of [26]hexaphyrin, the overall energy relaxation processes in its S_1 and T_1 states are less sensitive to the temperature change because of its relatively rigid and planar structure and Hückel aromatic $[4n+2]\pi$ electronic system. In contrast, [28]hexaphyrin reveals more temperature-sensitive behavior due to the interconversion processes between the two accessible conformers with planar/distorted Möbius topologies.

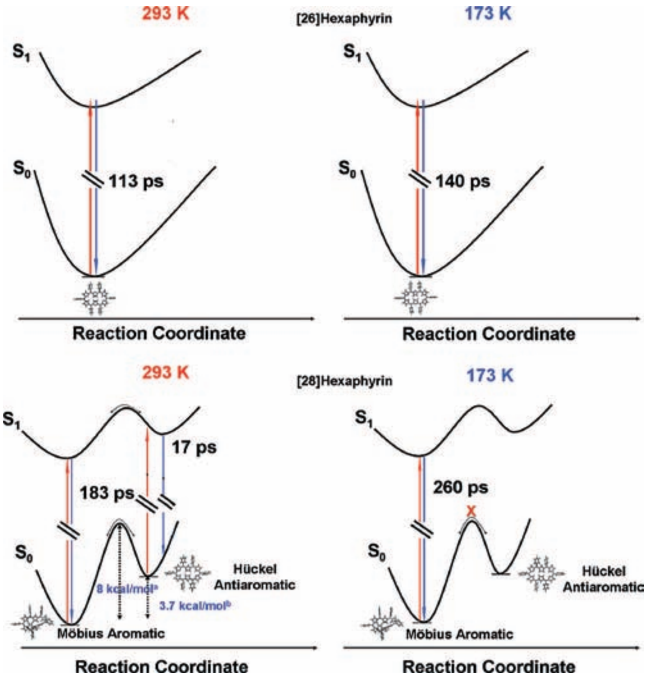

Figure 7. Schematic diagram for the energy relaxation pathways of [26] and [28]hexaphyrins: (a) Activation energy is calculated by dynamic NMR method from temperature-dependent ^{13}C, ^{1}H NMR spectra. (b) Estimated from the total energy difference between Möbius aromatic and Hückel antiaromatic [28]hexaphyrin, using the Gaussian 03 program.

Generally, nonplanar porphyrins exhibit much broader optical spectra, larger Stokes shifts, and stronger temperature-dependent behaviors due to their conformational flexibilities in the solution phase. Holten et al.[31-34] reported that the photophysical properties of nonplanar porphyrins (saddled and ruffled structures) are quite different from those of planar porphyrins (H_2TPP, H_2OEP, etc.). On the basis of this work, it has been generally accepted that most nonplanar porphyrins (saddled and ruffled types) exhibit shorter excited state lifetimes than planar porphyrins.[31−34] In spite of its nonplanar geometry, however, the lifetimes of distorted Möbius aromatic [28]hexaphyrin in the singlet and triplet excited states are longer than those of planar Hückel aromatic [26]hexaphyrin. To explain these interesting observations for [28]hexaphyrin, we have considered two points of view: one is the enhancement of rigidity by conformational constraints and the other is the degree of aromaticity of Möbius [28]hexaphyrin.

Owing to the fact that the excited state lifetimes for [28]hexaphyrin increase as the temperature decreases, we suggest that the potential energy surface of Möbius aromatic [28]hexaphyrin in both ground and singlet excited states has a narrower curvature than that of Hückel aromatic [26]hexaphyrin. Namely, they have a narrower potential well with larger force constants (Hessian). As a consequence, the Möbius structure of [28]hexaphyrin would experience more constrained molecular motions. In other words, upon lowering the temperature, [28]hexaphyrin becomes locked into the structures with Möbius topology which are more stable and rigid.

According to the previous studies on various expanded porphyrins, the excited singlet and triplet states of most aromatic expanded porphyrins have longer lifetimes than their corresponding antiaromatic congeners.[5,24−26] Thus, we think that the degree of aromaticity of expanded porphyrin could be a parameter to be strongly associated with the excited state dynamics. As described in the Introduction, Möbius [28]hexaphyrin shows a large negative NICS value (−15.1), large HOMA (0.85) value, and nearly degenerate HOMO and LUMO orbitals (see Figure S7 in the SI), which support the aromatic character of Möbius [28]hexaphyrin.

Furthermore, the TPA cross-section value is another experimental factor to be considered as the degree of aromaticity of expanded porphyrins. It should be noted that the previous reports by Cho et al.,[35,36] involving a series of octupolar electron donor−acceptor molecular systems, also conclude that the first hyperpolarizability (β) is linearly proportional to the TPA cross-section values. Although these workers did not directly mention the correlation between hyperpolarizability and BLA (bond length alternation, one of the classic indices of aromaticity) or between the hyperpolarizabilities, we can infer from their results that the imaginary part of γ (the second-order hyperpolarizability) determines the TPA cross-section values. In even earlier work, Brédas et al.[37] showed that the BLA is an essential parameter and a key determinant of the NLO response exhibited by conjugated organic molecules. Consistent with both of the above theoretical studies, our experimental results demonstrate a close relationship between the TPA cross-section values and the aromaticity as reflected in the second-order hyperpolarizabilities in the present set of [26]- and [28]hexaphyrins. In other words, the TPA cross-section value and the aromaticity are related in terms of both molecular hyperpolarizability and ring current. Thus, independent of what baseline criterion is chosen to define the aromaticity, the TPA cross-section values provide a useful experimental measure of the aromaticity.

In this regard, the large increase in the TPA cross-section values at lower temperature clearly indicates that the degree of aromaticity increases in [28]hexaphyrins as temperature decreases. We believe that this feature is attributable to the energetic stabilization through conformational changes from the planar antiaromatic structures to the Möbius topology ones in [28]hexaphyrins.

Another interesting point is that the TPA value of Möbius [28]hexaphyrin (9100 GM) at 173 K is almost two times as large as those of group 10 metal coordinated Möbius aromatic [28]hexaphyrins (4600−5500 GM). It should be noted that the dihedral angle between most distorted pyrroles is smaller in Möbius [28]hexaphyrin (~26.5°) compared with metal coordinated ones (39.9−45.8°),[12] and a small dihedral angle allows efficient π electron conjugation. Thus, these observations indicate that the structure of Möbius [28]hexaphyrin formed at low temperature reveals more smooth and less strained Möbius topology than metal coordinated ones. Furthermore, the TPA values of Möbius [28]hexaphyrin are comparable to those of Hückel aromatic [26]hexaphyrins, which illustrates that the degree of aromaticity for Möbius [28]hexaphyrin is nearly the same as that of Hückel aromatic [26]hexaphyrin.

To design Möbius aromatic molecules, a proper ring size of π-conjugated macrocycle is an important parameter to be considered. Herges et al.[7] demonstrated that small twisted cyclic molecules are difficult to realize stable Möbius topology due to large ring strains. In contrast, in larger cyclic [4*n*] annulene molecules, ring strain is less pronounced but the overall structures are very flexible and flip back to the less-strained Hückel topology. Thus, locking into the twisted Möbius structure is hard to accomplish.

Through small dihedral angles and large TPA values of Möbius [28]hexaphyrin, we can suggest that Möbius [28]hexaphyrin has a suitable ring size and smooth topology to realize the stable Möbius aromatic molecule with optimal π-electron delocalization. Thus, a subtle balance between energetic stabilization by π-electron delocalization and the strains induced by distorted Möbius structure occurs in Möbius [28]hexaphyrin as the temperature decreases. Additionally, once the rigid and stable molecular structure of Möbius [28]hexaphyrin is locked at low temperature, it gives rise to longer S_1 and T_1 state lifetimes. Overall, our study is the first spectroscopic investigation on stable Möbius aromatic expanded porphyrins without the assistance of central metal coordination in the formation of Möbius structures.

Summary

From the temperature-dependent spectroscopic studies of [26]- and [28]hexaphyrins, we have observed that while [26]hexaphyrin shows nearly temperature-independent behavior indicating a relatively planar structure, [28]hexaphyrin exhibits the conformational interconversion from planar Hückel antiaromatic structures to distorted Möbius aromatic ones as the temperature decreases.

Especially, upon lowering the temperature, [28]hexaphyrin reveals the distinct Möbius aromaticity with optimal π-electron delocalization as evidenced by smaller dihedral angles and larger TPA cross-section values compared with metalated Möbius [28]hexaphyrin. These observations indicate that [28]hexaphyrin exhibits a balance between a suitable ring size, which minimizes the distortional strains, and energy stabilization by π-electron delocalization to sustain the stable and rigid Möbius topology. Therefore, once the Möbius structure of [28]hexaphyrin is locked at low temperatures, the S_1 and T_1 state lifetimes become longer due to the rigidity and stability of Möbius structures. Through our study, we believe that we are able to provide useful information on the structure/property relationships of Möbius aromatic expanded porphyrins.

Acknowledgment. The work at Yonsei University was financially supported by the Star Faculty and World Class University Programs of the Ministry of Education, Science and Technology and the AFSOR/AOARD grant (No. FA4869-08-

1-4097). The work at Kyoto University was supported by Grant-in-Aids for Scientific Research (Nos. 19205006 and 18655013) from MEXT. Work at Northwestern University was supported by the Chemical Sciences, Geosciences, and Biosciences Division, Office of Basic Energy Sciences, DOE under grant no. DE-FG02-99ER14999. K.S.K, Z.S.Y, and J.Y.S acknowledges the fellowship of the BK 21 program from the Ministry of Education, Science and Technology of Korea. S.M., J.S., and S.S. acknowledge the fellowship from JSPS. The quantum calculations were performed by using the supercomputing resource of the Korea Institute of Science and Technology Information (KISTI)

Supporting Information Available: SMCR analysis of [28]hexaphyrin, temperature-dependent changes in Stokes shifts and relative fluorescence quantum yields, temperature-dependent femtosecond transient absorption decay profiles of [28]hexaphyrin, variable-temperature ^{13}C and ^{1}H NMR spectra and Arrehenius plots of [28]hexaphyrin, and a schematic molecular orbital diagram. This material is available free of charge via the Internet at http://pubs.acs.org.

References and Notes

(1) Shin, J.-Y.; Furuta, H.; Yoza, K.; Igarashi, S.; Osuka, A. *J. Am. Chem. Soc.* **2001**, *123*, 7190–7191.

(2) Suzuki, M.; Osuka, A. *Org. Lett.* **2003**, *5*, 3943–3946.

(3) Neves, M. G. P. M. S.; Martins, R. M.; Tomé, A. C.; Silvestre, A. J. D.; Silva, A. M. S.; Félix, V.; Drew, M. G. B.; Cavaleiro, J. A. S. *Chem. Commun.* **1999**, 385–386.

(4) Ahn, T. K.; Kwon, J. H.; Kim, D. Y.; Cho, D. W.; Jeong, D. H.; Kim, S. K.; Suzuki, M.; Shimizu, S.; Osuka, A.; Kim, D. *J. Am. Chem. Soc.* **2005**, *127*, 12856–12861.

(5) Yoon, Z. S.; Kwon, J. H.; Yoon, M.-C.; Koh, M. K.; Noh, S. B.; Sessler, J. L.; Lee, J. T.; Seidel, D.; Aguilar, A.; Shimizu, S.; Suzuki, M.; Osuka, A.; Kim, D. *J. Am. Chem. Soc.* **2006**, *128*, 14128–14134.

(6) Kwon, J. H.; Ahn, T. K.; Yoon, M. C.; Kim, D. Y.; Koh, M. K.; Kim, D.; Furuta, H.; Suzuki, M.; Osuka, A. *J. Phys. Chem. B* **2006**, *110*, 11683–11690.

(7) Ajami, D.; Oeckler, O.; Simon, A.; Herges, R. *Nature* **2003**, *426*, 819–821.

(8) Heilbronner, E. *Tetrahedron Lett.* **1964**, *5*, 1923–1928.

(9) Zimmerman, H. E. *J. Am. Chem. Soc.* **1966**, *88*, 1564–1565.

(10) Moll, J. F.; Pemberton, R. P.; Gutierrez, M. G.; Castro, C.; Karney, W. L. *J. Am. Chem. Soc.* **2007**, *129*, 274–275.

(11) Stêpień, M.; Latos-Grażyński, L.; Sprutta, N.; Chwalisz, P.; Szterenberg, L. *Angew. Chem., Int. Ed.* **2007**, *46*, 7869–7871.

(12) Rzepa, H. S. *Org. Lett.* **2008**, *10*, 949–952.

(13) Pacholska-Dudziak, E.; Skonieczny, J.; Pawlicki, M.; Szterenberg, L.; Ciunik, Z.; Latos-Grażyński, L. *J. Am. Chem. Soc.* **2008**, *130*, 6182–6195.

(14) Tanaka, Y.; Saito, S.; Mori, S.; Aratani, N.; Shinokubo, H.; Shibata, N.; Higuchi, Y.; Yoon, Z. S.; Kim, K. S.; Noh, S. B.; Park, J. K.; Kim, D.; Osuka, A. *Angew. Chem., Int. Ed.* **2008**, *47*, 681–683.

(15) Park, J. K.; Yoon, Z. S.; Yoon, M.-C.; Kim, K. S.; Mori, S.; Shin, J.-Y.; Osuka, A.; Kim, D. *J. Am. Chem. Soc.* **2008**, *130*, 1824–1825.

(16) Sankar, J.; Mori, S.; Saito, S.; Rath, H.; Suzuki, M.; Inokuma, Y.; Shinokubo, H.; Kim, K. S.; Yoon, Z. S.; Shin, J.-Y.; Lim, J. M.; Matsuzaki, Y.; Matsushita, O.; Muranaka, A.; Kobayashi, N.; Kim, D.; Osuka, A. *J. Am. Chem. Soc.* **2008**, *130*, 13568–13579.

(17) Greenfield, S. R.; Wasielewski, M. R. *Opt. Lett.* **1995**, *20*, 1394–1396.

(18) Noda, I.; Dowrey, A. E.; Marcott, C.; Story, G. M.; Ozaki, Y. *Appl. Spectrosc.* **2000**, *54*, 236A–248A.

(19) Jung, Y. M.; Noda, I. *Appl. Spectrosc. Rev.* **2006**, *41*, 515–547.

(20) Jung, Y. M.; Noda, I.; Kim, S. B. *Appl. Spctrosc.* **2003**, *57*, 1376–1380.

(21) Mori, S.; Osuka, A. *J. Am. Chem. Soc.* **2005**, *127*, 8030–8031.

(22) Mori, S.; Kim, K. S.; Yoon, Z. S.; Noh, S. B.; Kim, D.; Osuka, A. *J. Am. Chem. Soc.* **2007**, *129*, 11344–11345.

(23) Rybtchinski, B.; Sinks, L. E.; Wasielewski, M. R. *J. Phys. Chem. A* **2004**, *108*, 7497–7505.

(24) Yoon, Z. S.; Cho, D.-G.; Kim, K. S.; Sessler, J. L.; Kim, D. *J. Am. Chem. Soc.* **2008**, *130*, 6930–6931.

(25) Yoon, Z. S.; Noh, S. B.; Cho, D.-G.; Sessler, J. L.; Kim, D. *Chem. Commun.* **2007**, 3378–3380.

(26) Lament, B.; Dobkowski, J.; Sessler, J. L.; Weghorn, S. J.; Waluk, J. *Chem. Eur. J.* **1999**, *5*, 3039–3045.

(27) Song, N. W.; Cho, H. S.; Yoon, M. C.; Aratani, N.; Osuka, A.; Kim, D. *Bull. Korean Soc.* **2002**, *23*, 271–276.

(28) Sheik-Bahae, M.; Said, A. A.; Wei, T.-H.; Hagan, D. G.; van Stryland, E. W. *IEEE J. Quantum Electron.* **1990**, *26*, 760–769.

(29) Jackman, L. M.; Cotton, F. A., Eds. *Dynamic Nuclear Magnetic Resonance Spectroscopy*; Academic Press: New York, 1975.

(30) Frisch, M. J.; Trucks, G. W.; Schlegel, H. B.; Scuseria, G. E.; Robb, M. A.; Cheeseman, J. R.; Montgomery, J. A., Jr.; Vreven, T.; Kudin, K. N.; Burant, J. C.; Millam, J. M.; Iyengar, S. S.; Tomasi, J.; Barone, V.; Mennucci, B.; Cossi, M.; Scalmani, G.; Rega, N.; Petersson, G. A.; Nakatsuji, H.; Hada, M.; Ehara, M.; Toyota, K.; Fukuda, R.; Hasegawa, J.; Ishida, M.; Nakajima, T.; Honda, Y.; Kitao, O.; Nakai, H.; Klene, M.; Li, X.; Knox, J. E.; Hratchian, H. P.; Cross, J. B.; Bakken, V.; Adamo, C.; Jaramillo, J.; Gomperts, R.; Stratmann, R. E.; Yazyev, O.; Austin, A. J.; Cammi, R.; Pomelli, C.; Ochterski, J. W.; Ayala, P. Y.; Morokuma, K.; Voth, G. A.; Salvador, P.; Dannenberg, J. J.; Zakrzewski, V. G.; Dapprich, S.; Daniels, A. D.; Strain, M. C.; Farkas, O.; Malick, D. K.; Rabuck, A. D.; Raghavachari, K.; Foresman, J. B.; Ortiz, J. V.; Cui, Q.; Baboul, A. G.; Clifford, S.; Cioslowski, J.; Stefanov, B. B.; Liu, G.; Liashenko, A.; Piskorz, P.; Komaromi, I.; Martin, R. L.; Fox, D. J.; Keith, T.; Al-Laham, M. A.; Peng, C. Y.; Nanayakkara, A.; Challacombe, M.; Gill, P. M. W.; Johnson, B.; Chen, W.; Wong, M. W.; Gonzalez, C.; Pople, J. A. *Gaussian 03*; Gaussian, Inc.: Pittsburgh, PA, 2003.

(31) Chirvony, V. S.; Hoek, A.; Galievsky, V. A.; Sazanovich, I. V.; Schaafsma, T. J.; Holten, D. *J. Phys. Chem. B* **2000**, *104*, 9909–9917.

(32) Gentemann, S.; Medforth, C. J.; Forsyth, T. P.; Nurco, D. J.; Smith, K. M.; Fajer, J.; Holten, D. *J. Am. Chem. Soc.* **1994**, *116*, 7363–7368.

(33) Gentemann, S.; Nelson, N. Y.; Jaquinod, L.; Nurco, D. J.; Leung, S. H.; Medforth, C. J.; Smith, K. M.; Fajer, J.; Holten, D. *J. Phys. Chem. B* **1997**, *101*, 1247–1254.

(34) Song, H.-E.; Cissell, J. A.; Vaid, T. P.; Holten, D. *J. Phys. Chem. B* **2007**, *111*, 2138–2142.

(35) Lee, H.; An, S.-Y.; Cho, M. *J. Phys. Chem. B* **1999**, *103*, 4992–4996.

(36) Lee, W.-H.; Lee, H.; Kim, J.-A.; Choi, J.-H.; Cho, M.; Jeon, S.-J.; Cho, B. R. *J. Am. Chem. Soc.* **2001**, *123*, 10658–10667.

(37) Meyers, F.; Marder, S. R.; Pierce, B. M.; Brédas, J. L. *J. Am. Chem. Soc.* **1994**, *116*, 10703–10714.

JP8111205